59

Egypt. J. Chem. **Vol. 67**, No. 2. pp. 113 - 124 (2024)

Egyptian Journal of Chemistry

http://ejchem.journals.ekb.eg/

Judd-Ofelt Analysis and Spectroscopic Investigation for doped Nd3+ lead phosphate Zinc glasses

Aly Okasha[a,*] , Samir Y. Marzouk[b]

[a] *Spectroscopy Department, Physics Institute, National Research Centre, 33 ElBehouth St., Dokki, 12311 Giza, Egypt.*

[b] *Basic and Applied Science Department, College of Engineering and Technology, Arab Academy for Science, Technology and Maritime Transport, Cairo, Egypt*

Abstract

In this paper, a neodymium-doped Lead-Phosphate-Zinc glass system is prepared using melt–quenching technique. The samples are prepared using the nominal composition (70-x) P2O3-25PbO-10ZnO-(x) Nd2O3, where x = 0, 1, 1.5, 2, and 2.5 mol%. With increasing Nd2O3 content, the produced glasses' density and molar volume were evaluated. The absorption transitions from the ground state 4I9/2 to the different excited states were assigned using UV-Vis spectroscopy. The emission transitions from 4F3/2 ground state to 4I9/2, 4I9/11, and 4I9/13 excited states were measured using a spectrofluorometer; using Raman spectroscopy, the structure of the glasses samples was discussed. The Judd-Ofelt theory estimated the intensity parameter and the optical transitions of Nd3+ ions. The analyzed J-O intensity parameters followed the pattern Ω2 > Ω6 > Ω4. The lifetime values show that the glasses are suitable for laser applications. In addition, the findings show that the current glasses samples are good candidates for optoelectronic applications, especially in the optical communication band at 1064 nm.

Keywords: Nd3+; Judd-Ofelt; Lead Phosphate glass; Absorption; Emission; Raman

1. Introduction

Recently, Rare earth oxide materials (RE'O) have been essential dopants for other materials like glass. RE'O materials are necessary for their use in various applications, such as display devices, sensors, optical fibers, optical amplifiers, and telecommunications [1]. Among RE'O, Neodymium (Nd3+) is essential in fabricating laser materials due to its broad emission cross-section in the infrared spectral region and strong absorption in the visible region. Choosing the host glasses materials is essential in tailoring the preferred optical properties for specific applications. Borate [2], Phosphate [3,4], Silicate [5], and Telluride [6] glasses were employed as host materials for investigation or to produce targeted optical properties. In contrast, I. Kotb et al. [2] investigate the effect of adding (strontium oxide SrO and tungsten oxide WO3) to Borate host glasses. A.A. El-Maaref et al. [4] studied the optical and radiative properties of Phosphate glasses host material in the presence of (Zinc oxide ZnO and Sodium Carbonate Na2CO3. Y. Zhang et al. studied the infrared emission from Telluride glasses in the presence of (ZnO and Calcium oxide CaO) [6]. Researchers used different host materials and added serval modifiers to improve the resultant optical properties, especially for producing infrared emission from the Nd3+ ions doped glasses. Most results concentrate on near-infrared (NIR) quality around 1064 nm.

Using Lead oxide (PbO) as a former or modifier usually concentrate on different kind of radiation shielding [7–11], photon attenuation [12], and electromagnetic ray absorber [13] applications. The role of PbO depends on its %mol content in the glasses mixture and the type of bonding between oxygen and Lead [14]. It was discovered that Pb2+ ions occupy a

*Corresponding author e-mail: aliokasha2@yahoo.com; (Aly Okasha)

Received date 12 June 2023; revised date 17 July 2023; accepted date 31 July 2023

DOI: 10.21608/ejchem.2023.217283.8130

position between P-O-P layers in PbO-P2O5 glasses beside the presence of the P=O group in the polyhedron of the lead [8]. On the other hand, adding ZnO as a glass modifier due to its wide band gap may control the optical properties of the glasses and increase its chemical stability due to the formation of f P–O–Zn ionic bond [15–17].

Recently, Judd-Ofelt (J-O) analysis was wildly used to predict some optical parameters of glasses materials. Applying this analysis to the glass parameters obtained from the absorption data leads to estimating the intensities of different allowed transitions. Ω_2,Ω_4,and Ω_6 are the three intensity parameter obtained from J-O calculations. Ω_2, gives information about the effect of the surrounding environment on the RE'O [18,19]. Ω_2 and Ω_4, both give information about the rigidity of the glasses [2,20–24].

In the present work, PbO and ZnO first modified phosphate glasses, and then they were doped with Nd2O3. This was done to evaluate the host glass's influence and its modifiers' influence on the optical characteristics, particularly the emission at 1064 nm for Photonics materials candidates.

2. Experimental work

2.1. Samples preparation

Nd_2O_3 was purchased from (Sisco Research Lab. India), while P_2O_5, PbO, and ZnO from (Laboratory Rasayan Sd Fine Chem. Limited). The sample preparation was described elsewhere in the group's previous work [25]. The chemicals were used in powder form as received without further purification in a typical preparation method.

For the preparation of the glass samples, the melt-quenching technique was used. To get a high level of homogeneity, the mixes of the precursors, each weighing 35 g, were carefully combined in porcelain crucibles before being placed in an electrical furnace set to 1100 ±10 ºC for one hour. During this time, the melt was rotated once every 30 minutes. The molten metal was poured into a mold made of a custom-designed stainless steel template that measured 4 cm, 9 mm, and 9 mm. The mold was then sintered for thirty minutes at 300 ºC Celsius. After completing the last step, the samples were allowed to reach room temperature at a pace of thirty degrees Celsius each hour. Six samples were named Nd1 to Nd6 in addition to the base sample. All samples were polished and kept for further investigation.

2.2. Molar and Volume Density calculations

The glass density, denoted by the symbol (ρ), was determined using the Archimedes technique, assuming that the density of xylene liquid is equal to 0.863 g/cm3. The mutual glass density approximates the molar glass volume or Vm. The experiment was carried out several times, and a record of the density's average value was kept each time. T

2.3. Uv-Vis- NIR Absorption measurements

The optical absorption Spectra for the studied samples were carried out using JASCO (Japan) spectrophotometer Model V-770 UV–VIS-NIR spectrometer at room temperature. The spectra were measured from 300 nm up to 2750 nm.

2.4. Emission spectra measurements

The emission spectra for selected samples were carried out using a Spectrofluorometer (Model FS5, Edinburgh Instruments, UK) equipped with Fluoracle® software from 800 nm to 1600 nm, using 532 nm excitation wavelength.

2.5. Raman scattering analysis

Confocal micro Raman microscope OXFORD (Witec-Germany) Model Alpha 300 equipped with Nd-Yag laser of variable power output and control five software was used to record the Raman scattering spectra for four samples, the base, Nd1, Nd3, and Nd6. 532 nm excitation wavelength was used during measurements with 30 mW laser power in the spectral range from 100 cm-1 to 2500 cm-1.

3. Results and Discussion

3.1. Density and molar volume calculations

The sample density is calculated using Archmidis's method from the following equation:

$$\rho = W_{air}/(W_{air}-W_{xylene}) \ x \ \rho_{xylene} \quad (1)$$

Where W_{air} and W_{xylene} are the weight of the sample in air, and the weight of xylene, and ρ_{xylene} is the density of xylene (0.863 g/cm3).

The Molar volume of the sample is calculated using the equation:

V_M=M/ρ (2)

N_i=(xρN_A)/M (3)

R=(1/N_i)^(1/3) (4)

Where M, Ni, and R are the molecular weight, the concentration of Nd_2O_3 and the mean Nd^{3+} ions separation.

The Calculated density and Molar volume of the samples under investigation were illustrated in Table (1) and Fig. (1), where it can be noticed that there are inversely proportional between the density and the Molar Volume. That means the ionic groups are firmly connected, and the sample has high compactness [26]. Due to the higher molecular weight of the Nd2O= (336.477 g.mol-1) rather than the P2O5 (141.943 g.mol-1) and also the of the Nd3+ ionic radii, the increase in RE'O in the sample gradually produces more non-bridging Oxygen which leads to applying the modification to the glass network [27].

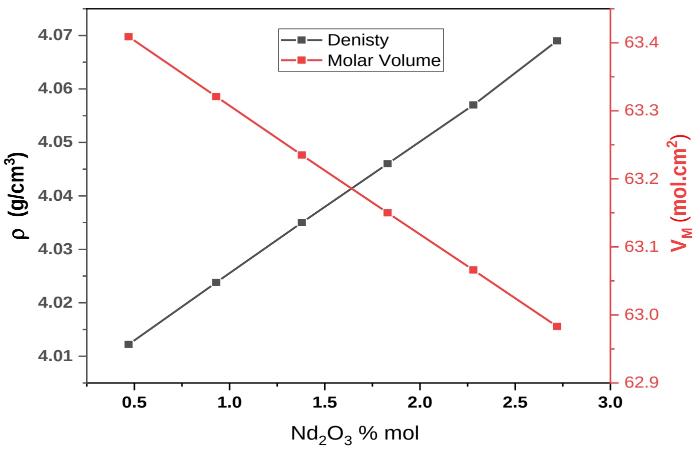

Figure (1). The changes in Density and Molar Volume with the Nd_2O_3 % mol

3.2. Optical Absorption

The data from the optical absorption experiments are shown in Figure (2). Figure (2-a) represents the range that extends from 200 nm to 1000 nm, and Figure (2-b) represents the range that extends from 1000 nm to 2750 nm. The range was broken up into these two figures for transparency. The optical transitions seen in absorption spectra are caused by the excitation of the $^4I_{9/2}$ ground state.

Table 1: The mole fraction, glass density, ρ, molar volume, V_m, Nd^{3+} ion concentration N, and mean Nd^{3+} ion separation, R for the studied samples.

Glass	Composition mol.%				ρ (gm/cm^3) ±0.04	V_M (mol.cm^3) ±0.0.28	N X10^{20}	R(nm)
	P_2O_5	PbO	ZnO	Nd_2O_3				
Nd 0	65.95	24.47	9.58		3.999	63.524	0	0
Nd 1	65.64	24.35	9.54	0.47	4.0122	63.409	0.88	225.09
Nd 2	65.34	24.24	9.49	0.93	4.0238	63.321	1.75	178.85
Nd 3	65.04	24.13	9.45	1.38	4.035	63.235	2.61	156.41
Nd 4	64.74	24.02	9.41	1.83	4.046	63.150	3.47	142.26
Nd 5	64.45	23.91	9.36	2.28	4.057	63.066	4.33	132.20
Nd 6	64.16	23.80	9.32	2.72	4.069	62.983	5.18	124.54

Table 2: Absorption transitions for studied glasses samples

From $^4I_{9/2} \rightarrow$ To	Wavelength (nm)
$^4D_{7/2}$	320
$^4D_{5/2}+^4D_{3/2}$	320
$^4D_{5/2}+^4D_{3/2}$	352
$^4P_{1/2}$	428
$^2G_{3/2}+^4G_{9/2}+^4K_{15/2}$	472
$^4G_{7/2}$	522
$^4G_{5/2}+^4G_{7/2}$	580
$^3H_{11/2}$	628
$^4F_{9/2}$	682
$^4F_{7/2}+^4S_{3/2}$	744
$^4F_{5/2}+^4H_{9/2}$	802
$^4F_{3/2}$	874
$^4I_{15/2}$	1608
$^4I_{13/2}$	2436

Several sublevel excited states[27], described in Table 2, along with the wavelengths that correspond to them [28–33]. The line 4I9/2 → 4G5/2+4G7/2 is the hypersensitive transition (HST) [4,29], occurring when 4I9/2 is excited to 4G5/2+4G7/2. When there is a greater concentration of Nd3+ in the samples, there is a corresponding rise in the relative intensity of all transitions.

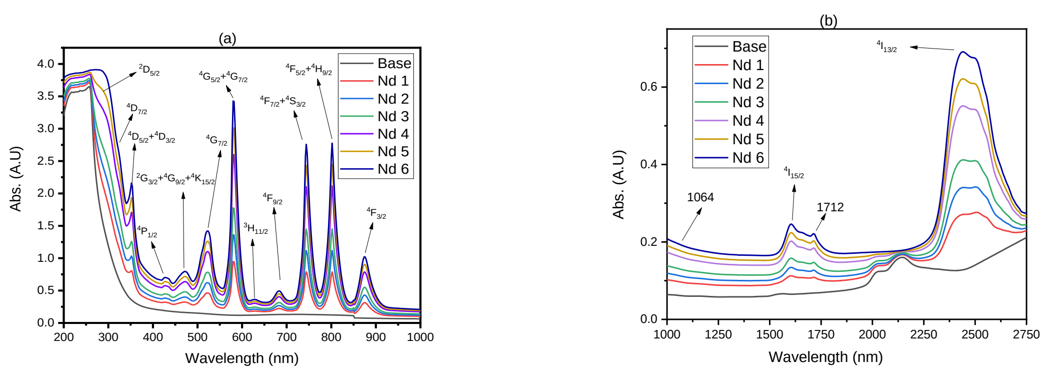

Figure 2: Optical absorption transitions in the range (a) from 350nm to 1000 nm and (b) from 1300 nm to 2800 nm.

3.3. Optical band gap estimation

Investigating the primary absorption edge in the UV-Vis range may acquire information regarding electronic band structure, optical transitions, and optical band gaps in amorphous materials. Glasses undergo both direct and indirect optical transitions as they approach the edge of their UV absorption spectrum. By absorbing energy from electromagnetic waves more significantly than the band gap energy, electrons that are now in the valence band have the potential to be stimulated into the conduction band. That results in indirect transitions. The band gap energy is calculated by equation [20,21,34] :

$$\alpha(\omega) = \alpha_o exp\left(\frac{h\omega}{\Delta E}\right) \quad (5)$$

Figure (3) represents Tauc's plot to illustrate the indirect gap for three samples Nd1, Nd3, and, Nd6, predicted from the extrapolation of the straight line of the relation between the photon energy (eV) and $ln(\alpha h\nu)^{0.5}$. The range of change in the indirect band gap with increasing the Nd^{3+} concentration is from 3.25 eV to 3.37 eV.

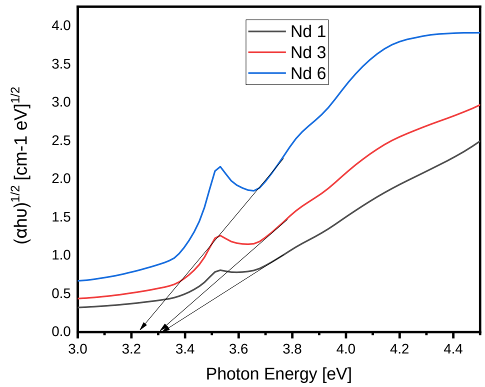

Figure 3: The Tauc's graph represents the indirect allowed transition for the selected glass sample.

3.4. Raman spectroscopy analysis

Phosphate glass has a characteristic Raman spectrum, as seen in Figure 4. Phosphate glasses are characterized by a structure that mostly contains Q_P^n groups of PO_4 tetrahedral (where n is the number of bridging oxygens excite in each PO4 tetrahedron) [35]. Previous studies divided the Phosphate Raman spectrum into two main sections. The first is located at 700 cm^{-1} and around wavenumbers [36]. The attribution of these peaks is due, in general, to the binding stretching of the phosphate units [35]. The second section is at 1200 cm^{-1} and around wavenumbers [37]. This region is attributed to the P–O stretching vibrations [35,36]. The Raman data of the studied samples are represented in Fig. 4. Five main bands are observed in the Base sample (Nd=0). The band at 327 cm^{-1} is attributed to PO_2 bending O-P-O bending motion [35–37]. By increasing the Nd^{3+} ions, this band shifted to 335 cm^{-1}. The addition of Nd^{3+} ions results in the de-polymerization of the phosphate glass network. This occurs due to the change of Q_P^2 structural units into Q_P^1 structural units and finally into Q_P^0 structural units. The band at 495 cm^{-1} is endorsed to O-P-O bending vibrations units, ν(PO2) modes of $(PO_2^-)^n$ chain groups [35]. The band at 694 cm^{-1} has been related to the symmetric stretching of P–O–P links in both Q_P^2 and Q_P^1 building structural units. The band at 1163 cm^{-1} is due to PO_2 non-bridging oxygen symmetric stretching in Q^2 units ($\nu s(PO_2)$) [29,35,36,38]. This sharp and clear band has two shoulders. The left is located at 1066 cm-1, corresponding to the symmetric stretching of non-bridging oxygen of PO2 in Q^1 building units. The right shoulder is located at 1230 cm^{-1} which is attributed to the PO_3 group asymmetric stretching vibrations [29,35,38]. The strong and broadband at 1918 cm^{-1} detected in the spectra of all glasses contained Nd^{3+}, and its intensity is increased with the concentrations of Nd^{3+} ions. This band doesn't observe in the base sample, and there is no certain assignment, so it needs to be clarified and discussed. This band introduces a strong evidence of the effect of the Nd^{3+} on the structure of the glass network[40].

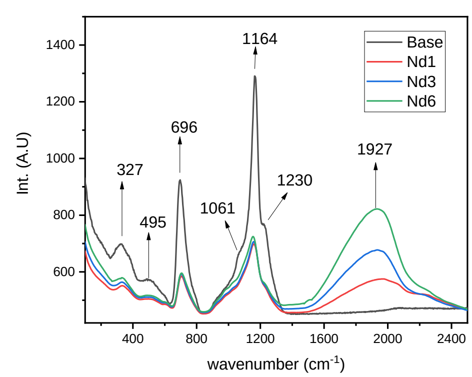

Figure 4: Raman spectra of glasses with different Nd_2O_3 concentration.

3.5. Emission Spectra for the Glasses

Figure (5) shows the emission spectra for Nd1, Nd3 and Nd6 samples in the spectral range from 800 nm to 1600 nm using the Yag laser line at 532 nm. The spectra represent the emission intensity as a function of Nd^{3+} concentrations. Three main transitions were observed owing to the transitions from $^4\mathbf{F}_{3/2}$ ground state to $^4\mathbf{I}_{9/2}$ (808 nm), $^4\mathbf{I}_{9/11}$ (1064 nm) and $^4\mathbf{I}_{9/13}$ (1385 nm) excited states and reported in previous work [33,41,42]. The transition corresponding to $^4\mathbf{F}_{3/2}\rightarrow{}^4\mathbf{I}_{9/11}$ is the most intense in the measured spectral range, and its intensity increases by increasing the Nd^{3+} ions concentrations.

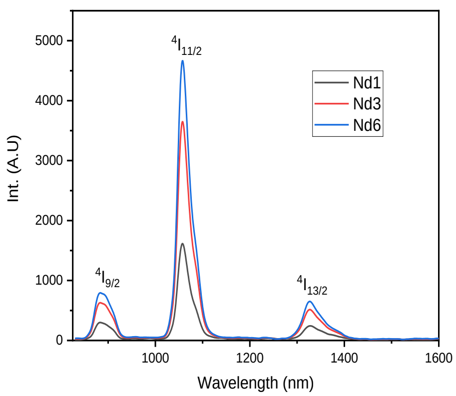

Figure 5: Emission spectra for Nd1, Nd3, and Nd6 glasses samples

3.6. Judd-Ofelt analysis

The (J–O) analysis can discuss whether the lasing is achievable and investigate the optical parameters that glasses provide. The radiative transition probability of Nd^{3+} ions was obtained by employing the J–O analysis to calculate the intensity of transitions in the current studied glasses using the J-O intensity parameters Ω_2, Ω_4, and Ω_6, which depend on the host glasses materials. The results of this calculation were then used to estimate the radiative transition probabilities of Nd^{3+} ions. The absorption bands are connected to the movement of electric dipoles and result from the electronic transitions between $4f \rightarrow 4f$ [4,33,41] . The oscillator strength, denoted by f_{exp}, is an indication of the intensity of the absorption transition and is measured by [2]

$$f_{exp} = 2.303 \frac{mc^2}{lN\pi e^2} \int \frac{OD(\lambda) d\lambda}{d\lambda^2} \quad (6)$$

where *l m, e, c, N and* OD(λ) are the thickness of the sample, m is the mass of the electron, e is the charge of the electron, c is the speed of light, N is the number of active ions per unit volume and OD(λ) is the optical density.

The oscillator strength predicted by the (J-O) theory (f_{cal}) for an electron to move from its ground state $(S, L)J$ to its excited state$(S', L')J'$, where the expression for J', is a function of the (J-O) parameters Ω_2, Ω_4 and Ω_6, is calculated using the formula [2,21]:

$$f_{cal}[(S,L)J;(S',L')J'] = \frac{8\pi^2 mc}{3h\lambda(2J+1)} \times \frac{(n^2+2)^2}{9n} \times \sum_{\lambda=2,4,6} \Omega_\lambda \left| \langle (S,L)J \rangle \middle\| U^\lambda \middle\| \langle (S',L')J' \rangle \right|^2 \quad (7)$$

Where, $\langle \| U^\lambda \| \rangle$ is the second order reduced of Weber tensor.

The mean square method fitting *(r.m.s)* may apply to the Uv-Vis absorption data to predict the (J-O) parameter intensities related to the Nd^{3+} conveyances. Using this method produces fitting accuracies regarding f_{exp} and f_{cal}, which may be approximated using the relation [21]:

$$r.m.s. = \left[\sum_P \frac{(f_{calc} - f_{meas})^2}{P-3} \right]^{\frac{1}{2}} \quad (8)$$

The parameter P denotes the detection quality of the absorption transitions.

Table (4) illustrates the calculating and experimental oscillator strengths f_{exp} and f_{cal} for the (J-O) parameters Ω_2, Ω_4 and Ω_6 at each absorption transition beside the (r.m.s) approximation values. The results obtained from Table (4) indicate that the transition at $^4\mathbf{I}_{9/2} \rightarrow {}^4\mathbf{G}_{7/2}$ is the most intense absorption transition, which agrees with measured absorption spectra by Uv-Vis data in Figure (2) ± 3 nm. In addition, the trend in the (J-O) is ($\Omega_2 > \Omega_6 > \Omega_4$) by means that the absorption transition is highly affected by the surrounding host glasses materials and has a good rigidity [21].

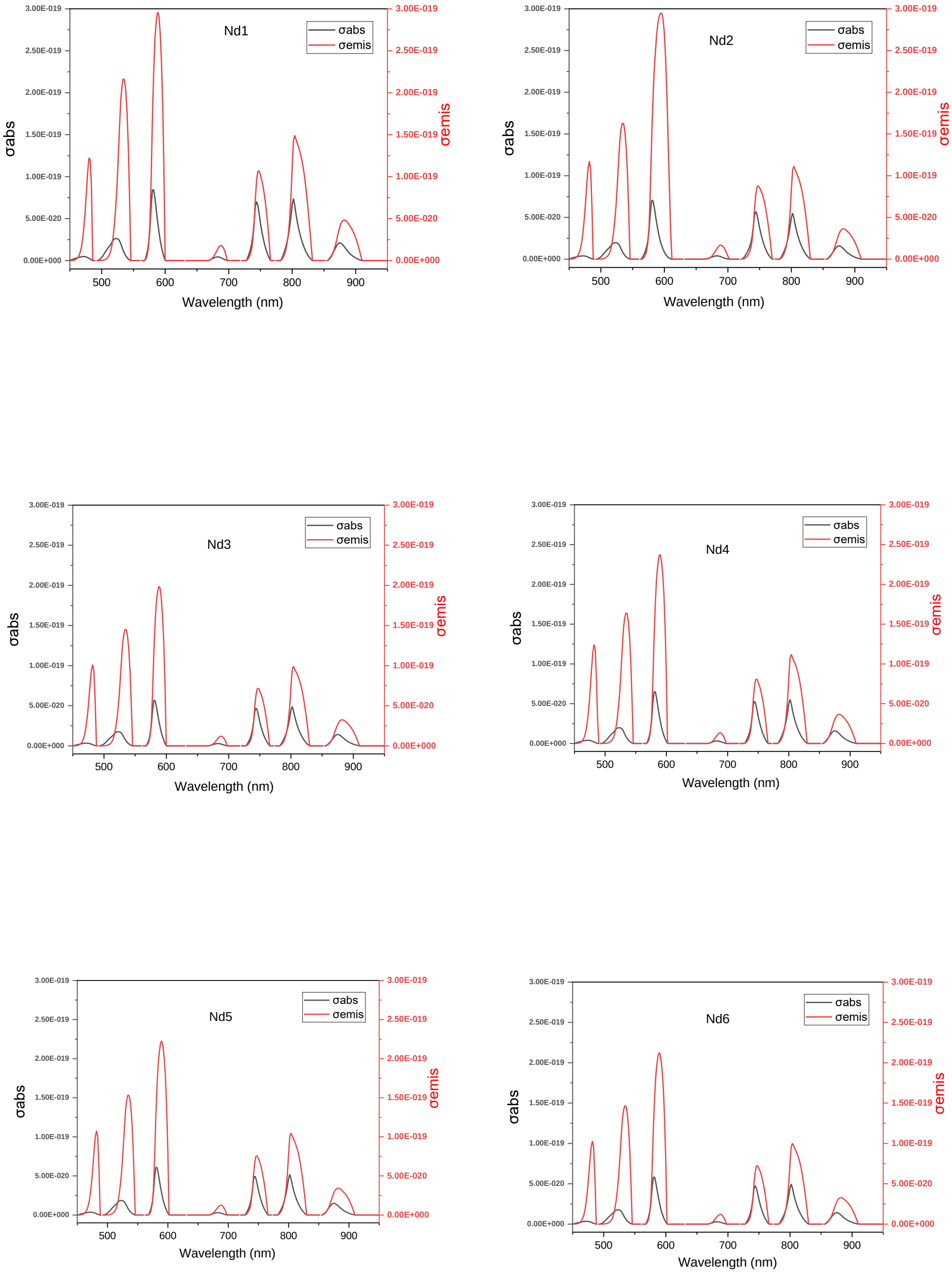

Figure 6: Estimated absorption cross section and Emission cross sections for the current studied glasses samples

Table 4: Measured and calculated absorption line strengths and J- O parameters Ω_λ of Nd^{3+} in (P_2O_5-PbO-ZnO-Nd_2O_3) glasses.

Transition $^4I_{9/2} \rightarrow$	**Wave-length (nm)**	**Energy (cm^{-1})**	**Nd 1**		**Nd 2**		**Nd 3**		**Nd 4**		**Nd 5**		**Nd 6**	
			f_{exp}	f_{cal}	f_{exp}	f_{cal}	f_{exp}	f_{cal}	f_{exp}	f_{cal}	f_{exp}	f_{cal}	f_{exp}	f_{cal}
			10^{-20} cm^2		**10^{-20} cm^2**		**10^{-20} cm^2**		**10^{-20} cm^2**		**10^{-20} cm^2**		**10^{-20} cm^2**	
$^4I_{13/2}$	2496	4005	4.5505	3.7032	3.0076	2.4973	2.1342	1.8367	1.65	1.6333	1.4475	1.412	1.3236	1.2985
$^4I_{15/2}$	1644	6080	0.6657	0.3713	0.3282	0.25	0.2415	0.1834	0.2277	0.1621	0.1992	0.1399	0.1799	0.1287
$^4F_{3/2}$	867	11527	0.6886	0.2004	0.4804	0.67	0.4233	0.0361	0.4717	0.2013	0.4326	0.209	0.4039	0.1986
$^4F_{5/2}$	795.	12573	1.7423	2.618	1.3013	1.8327	1.0662	1.4344	1.177	1.4453	1.0885	1.2846	1.0085	1.1878
$^4S_{3/2}$	742	13460	1.5696	1.9228	1.1189	1.2954	0.9423	0.951	1.0575	0.8424	0.9703	0.7276	0.9062	0.669
$^4F_{9/2}$	673	14854	0.176	0.3452	0.1189	0.235	0.1033	0.1778	1.135	0.1661	0.1035	0.1454	0.0965	0.1341
$^2G_{7/2}$	576	17333	2.5457	2.2908	1.7981	1.5863	1.5947	1.4036	1.7788	1.5708	1.6307	1.4325	1.525	1.3385
$^4G_{7/2}$	525	19018	1.5399	1.8724	1.0196	1.2995	0.8819	1.1366	0.9663	1.2622	0.8811	1.1489	0.8205	1.0726
Ω_2 (10^{-20} cm^2)			33.8005		22.6147		18.8517		19.2210		17.2285		16.0555	
Ω_4 (10^{-20} cm^2)			2.8371		1.6141		0.8119		0.212		0.1918		0.1859	
Ω_6 (10^{-20} cm^2)			8.2062		5.5250		4.0521		3.5809		3.0911		2.8417	
r. m. s. (10^{-20} cm^2)			0.7336		0.4509		4.0521		0.5031		0.2301		0.2161	

Using the estimated J-O parameters Ω_2, Ω_4 and Ω_6, many other parameters such as the lifetime of radiation (τ_r), the branching ratio (β_r), the absorption cross section (σ_{abs}), the emission cross section (σ_{emis}), Electric (*SED*) dipole strength, electric (*AED*) and magnetic (*AMD*) and radiative transition probabilities may evaluate from the equation:

$$A(J,J') = \frac{64\pi^2 e^2}{3h\lambda^3(2J+1)} \times \frac{n(n^2+2)^2}{9} \times \sum_{\lambda=2,4,6} \Omega_\lambda \left|\langle (S,L)J \rangle \left\| U^\lambda \right\| \langle (S',L')J' \rangle\right|^2 \quad (9)$$

Where,

$$\tau_{rad} = \frac{1}{\sum A(J,J')} \quad (10)$$

and,

$$\beta(J,J') = \frac{A(J,J')}{\sum_{J'} A(J,J')} \quad (11)$$

and,

$$\sigma_{emis}(\lambda) = \sigma_{abs}(\lambda) \frac{Z_l}{Z_u} exp\left[\frac{E_{Z_l} - hc\lambda^{-1}}{K_B T}\right] \quad (12)$$

and

$$\sigma_{abs}(\lambda) = 2.0303 \frac{OD(\lambda)}{Nl} \quad (13)$$

Table 5 Electric (S_{ED}) dipole strength, electric (A_{ED}) and magnetic (A_{MD}) radiative transition probabilities, branching ration (β_r), and radiative lifetime (τ_r) for Er-doped zinc-borate glass.

Glass symbol	Transition $^4I_{9/2} \rightarrow$	$S_{ED} \times 10^{-20}$ (cm^2)	A_{ED} (s^{-1})	A_{MD} (s^{-1})	β_r	τ_r (ms)	*n*
Nd 1	$^4I_{13/2}$	3.7032	22.087	0.000	0.6757	30.5941	1.33666
	$^4I_{15/2}$	0.3713	12.139	0.000	0.2182	17.9789	1.57101
	$^4F_{3/2}$	0.2004	239.970	0.000	0.1059	0.4412	1.69651
	$^4F_{5/2}$	2.6180	2781.382	0.000	0.7379	0.2653	1.70763
	$^4S_{3/2}$	1.9228	3831.543	0.000	0.4588	0.1197	1.71635
	$^4F_{9/2}$	0.3452	380.446	1.522	0.0854	0.2236	1.72916
	$^2G_{7/2}$	2.2908	5266.600	0.261	0.1783	0.0338	1.75251
	$^4G_{7/2}$	1.8724	5662.139	2.259	0.1085	0.0192	1.77117
Nd 2	$^4I_{13/2}$	2.4973	18.630	0.000	0.6677	35.8404	1.43848
	$^4I_{15/2}$	0.2500	9.784	0.000	0.2132	21.7950	1.65949
	$^4F_{3/2}$	0.0670	94.557	0.000	0.0489	0.5171	1.78017
	$^4F_{5/2}$	1.8327	2292.263	0.000	0.7306	0.3187	1.79109
	$^4S_{3/2}$	1.2954	3037.103	0.000	0.4678	0.1540	1.7997
	$^4F_{9/2}$	0.2350	304.542	1.753	0.0844	0.2757	1.81242
	$^2G_{7/2}$	1.5863	4284.315	0.300	0.1821	0.0425	1.83584
	$^4G_{7/2}$	1.2995	4614.958	2.595	0.1116	0.0242	1.85475
Nd 3	$^4I_{13/2}$	1.8367	13.788	0.000	0.6539	47.4220	1.44219
	$^4I_{15/2}$	0.1834	7.299	0.000	0.2102	28.7943	1.66812
	$^4F_{3/2}$	0.0361	52.044	0.000	0.0323	0.6203	1.79091
	$^4F_{5/2}$	1.4344	1832.181	0.000	0.7224	0.3943	1.80196
	$^4S_{3/2}$	0.9510	2277.339	0.000	0.4545	0.1996	1.81066
	$^4F_{9/2}$	0.1778	235.313	1.785	0.0839	0.3539	1.8235
	$^2G_{7/2}$	1.4036	3873.204	0.305	0.1899	0.049	1.8471
	$^4G_{7/2}$	1.1366	4124.856	2.643	0.1160	0.0281	1.86613
Nd 4	$^4I_{13/2}$	1.6333	12.643	0.000	0.6444	50.9683	1.45632
	$^4I_{15/2}$	0.1621	6.613	0.000	0.2066	31.2339	1.68039
	$^4F_{3/2}$	0.2013	296.655	0.000	0.1654	0.5576	1.80251
	$^4F_{5/2}$	1.4453	1887.666	0.000	0.7066	0.3743	1.81353
	$^4S_{3/2}$	0.8424	2062.661	0.000	0.4509	0.218	1.82222
	$^4F_{9/2}$	0.8424	2062.661	0.000	0.4509	0.218	1.83506
	$^2G_{7/2}$	1.5708	4431.166	0.311	0.2019	0.0456	1.85869
	$^4G_{7/2}$	1.2622	4682.561	2.692	0.1239	0.0264	1.87777
Nd 5	$^4I_{13/2}$	1.4120	11.685	0.000	0.6375	54.5516	1.48744
	$^4I_{15/2}$	0.1399	6.029	0.000	0.2039	33.825	1.70781
	$^4F_{3/2}$	0.1399	6.029	0.000	0.2039	33.825	1.82872
	$^4F_{5/2}$	1.2846	1764.264	0.000	0.7032	0.3986	1.83974
	$^4S_{3/2}$	0.7276	1873.175	0.000	0.4498	0.2401	1.84845
	$^4F_{9/2}$	0.1454	206.883	1.899	0.0815	0.3906	1.86135
	$^2G_{7/2}$	1.4325	4249.138	0.325	0.2042	0.0481	1.8852
	$^4G_{7/2}$	1.1489	4482.394	2.809	0.1254	0.0280	1.90453
Nd 6	$^4I_{13/2}$	1.2985	11.467	0.000	0.6338	55.2726	1.51792
	$^4I_{15/2}$	0.1287	5.847	0.000	0.2024	34.6099	1.7348
	$^4F_{3/2}$	0.1986	323.244	0.000	0.1948	0.6026	1.85458
	$^4F_{5/2}$	1.1878	1713.635	0.000	0.7024	0.4099	1.86559
	$^4S_{3/2}$	0.6690	1809.032	0.000	0.4494	0.2484	1.87432
	$^4F_{9/2}$	0.1341	200.436	1.979	0.0816	0.4029	1.88729
	$^2G_{7/2}$	1.3385	4170.704	0.338	0.2046	0.0491	1.91137
	$^4G_{7/2}$	1.0726	4396.603	2.928	0.1256	0.0285	1.93097

Using the calculated absorption cross section (σ_{abs}) and the emission cross section (σ_{emis}), the gain coefficient ($\sigma_{gain}(\lambda)$) could be estimated using the following equation [21]:

$$\sigma_{gain}(\lambda) = P\,\sigma_{emis}(\lambda) - (1 - P)\sigma_{abs}(\lambda) \qquad (14)$$

where P is the population inversion factor, where the gain cross section function was estimated by applying different population inversion values from P = 0 till P = 1 in 0.1 increasing steps and is presented in Figure 7, the function produced intensity increase gradually with the increase of the population inversion factor.

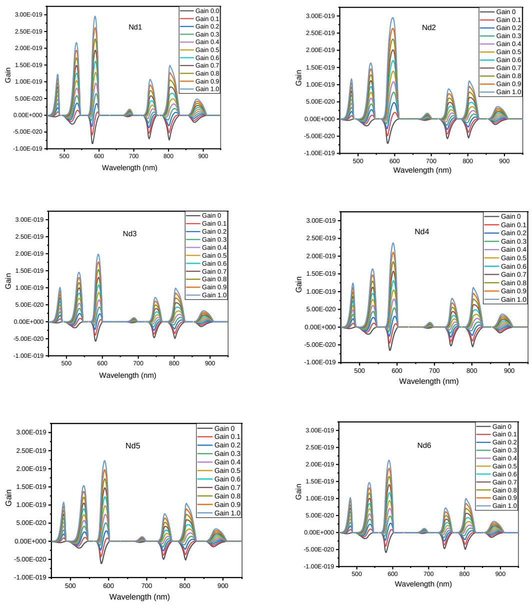

Figure 7: Gain coefficients σ_{gain} as a function of wavelength for the studied glasses samples

4. Conclusion

The nominal glasses with the targeted composition were successfully prepared. The optical absorption in UV-Vis range denoted transitions from the $^4F_{3/2}$ ground state to several excited states with (HST) at about 580 nm, which is confirmed by the estimated oscillator strength calculated by J-O analysis. The Raman shift reveals four bands associated with the vibration of the structural groups of the glasses. The strength of the peak at 1981 cm^{-1} increases with an increasing amount of Nd^{3+} ions present but cannot be pinpointed to a particular vibration and so needs to be investigated and clarified. The emission data collected show a significant transition at 1064 nm, which is utilized in the devices used for optical communications and optoelectronics applications. The J-O intensities characteristics have a $\Omega_2 > \Omega_6 > \Omega_4$ trend, which agrees with previous research. Additionally, the lifetime and branching ratio results support the recommendation of using the current glasses samples in optoelectronics and optical communications.

5. References

[1] S. Li, L. Zhou, H. Zhang, Investigation progresses of rare earth complexes as emitters or sensitizers in organic light-emitting diodes, Light Sci. Appl. 11 (2022). https://doi.org/10.1038/s41377-022-00866-w.

[2] I.E. Kotb, A. Okasha, S.Y. Marzouk, N.A. Zidan, Extensive study on the optical and structural characteristics of Nd3+ doped Lead-Borate-Strontium-Tungsten glass system: Judd–Ofelt analysis, Results Chem. 5 (2023) 100869. https://doi.org/10.1016/j.rechem.2023.100869.

[3] G. Neelima, K. Venkata Krishnaiah, N. Ravi, K. Suresh, K. Tyagarajan, T. Jayachandra Prasad, Investigation of optical and spectroscopic properties of neodymium-doped oxyfluoro-titania-phosphate glasses for laser applications, Scr. Mater. 162 (2019) 246–250. https://doi.org/10.1016/j.scriptamat.2018.11.018.

[4] A.A. El-Maaref, S. Badr, K.S. Shaaban, E.A. Abdel Wahab, M.M. ElOkr, Optical properties and radiative rates of Nd 3+ doped zinc-sodium phosphate glasses, J. Rare Earths. 37 (2019) 253–259. https://doi.org/10.1016/j.jre.2018.06.006.

[5] A.A. Menazea, A.M. Abdelghany, W.H. Osman, N.A. Hakeem, F.H.A. El-Kader, Precipitation of silver nanoparticles in silicate glasses via Nd:YAG nanosecond laser and its characterization, J. Non. Cryst. Solids. 513 (2019) 49–54. https://doi.org/10.1016/j.jnoncrysol.2019.03.018.

[6] Y. Zhang, L. Sun, Y. Chang, W. Li, C. Jiang, Multiband infrared luminescence of Er3+-Ho3+-Nd3+/Tm3+-codoped telluride glasses, Front. Optoelectron. 7 (2014) 74–76. https://doi.org/10.1007/s12200-013-0374-2.

[7] R. El-Mallawany, M.I. Sayyed, M.G. Dong, Y.S. Rammah, Simulation of radiation shielding properties of glasses contain PbO, Radiat. Phys. Chem. 151 (2018) 239–252. https://doi.org/10.1016/j.radphyschem.2018.06.035.

[8] K. El-Egili, H. Doweidar, Y.M. Moustafa, I. Abbas, Structure and some physical properties of PbO-P2O5 glasses, Phys. B Condens. Matter. 339 (2003) 237–245. https://doi.org/10.1016/j.physb.2003.07.005.

[9] D.K. Gaikwad, S.S. Obaid, M.I. Sayyed, R.R. Bhosale, V. V. Awasarmol, A. Kumar, M.D. Shirsat, P.P. Pawar, Comparative study of gamma ray shielding competence of WO3-TeO2-PbO glass system to different glasses and concretes, Mater. Chem. Phys. 213 (2018) 508–517. https://doi.org/10.1016/j.matchemphys.2018.04.019.

[10] B.M. Alotaibi, M.I. Sayyed, A. Kumar, M. Alotiby, A. Sharma, H.A. Al-yousef, N.A.M. Alsaif, Y. Al-hadeethi, Progress in Nuclear Energy Optical and gamma-ray shielding effectiveness of a newly fabricated P 2 O 5 – CaO

– Na 2 O – K 2 O – PbO glass system, 138 (2021).

[11] M.I. Sayyed, Y.S. Rammah, A.S. Abouhaswa, H.O. Tekin, B.O. Elbashir, ZnO-B2O3-PbO glasses: Synthesis and radiation shielding characterization, Phys. B Condens. Matter. 548 (2018) 20–26. https://doi.org/10.1016/j.physb.2018.08.024.

[12] H. Al-Ghamdi, M.I. Sayyed, M. Elsafi, A. Kumar, N. Al-Harbi, A.H. Almuqrin, S. Yasmin, M.U. Khandaker, An experimental study measuring the photon attenuation features of the P2O5–CaO–K2O–Na2O–PbO glass system, Radiat. Phys. Chem. 200 (2022). https://doi.org/10.1016/j.radphyschem.2022.110153.

[13] A. Taqi, A. Salih, A. Ibrahim, Electromagnetic-Ray Absorption Using B2O3-PbO-Na2O Glass Mixtures as Radiation Protection Shields, Arab J. Nucl. Sci. Appl. 0 (2021) 0–0. https://doi.org/10.21608/ajnsa.2021.74814.1469.

[14] F.A. Abdel-Wahab, A.M. Fayad, M. Abdel-Baki, H. AbdelMaksoud, Role of non-bridging oxygen defect in the ionic conductivity and associated oxygen trap centers in lead-borate oxide glass: Effect of structural substitution of PbO for Ag2O and Li2O modifiers, J. Non. Cryst. Solids. 500 (2018) 84–91. https://doi.org/10.1016/j.jnoncrysol.2018.06.033.

[15] M. Jerroudi, L. Bih, M. Azrour, B. Manoun, I. Saadoune, P. Lazor, Investigation of Novel Low Melting Phosphate Glasses Inside the Na2O–K2O–ZnO–P2O5 System, J. Inorg. Organomet. Polym. Mater. 30 (2020) 532–542. https://doi.org/10.1007/s10904-019-01213-0.

[16] C. Renuka, B. Sujatha, N. Sivasankarareddy, R. Viswanatha, C. Narayanareddy, Conductivity studies on molybdo-phosphate glasses containing ZnO, AIP Conf. Proc. 1942 (2018) 1–5. https://doi.org/10.1063/1.5029022.

[17] R. Oueslati-Omrani, A.H. Hamzaoui, Effect of ZnO incorporation on the structural, thermal and optical properties of phosphate based silicate glasses, Mater. Chem. Phys. 242 (2020) 122461. https://doi.org/10.1016/j.matchemphys.2019.122461.

[18] R. Reisfeld, G. Katz, N. Spector, C.K. Jørgensen, C. Jacoboni, R. De Pape, Optical transition probabilities of Er3+ in fluoride glasses, J. Solid State Chem. 41 (1982) 253–261. https://doi.org/10.1016/0022-4596(82)90143-8.

[19] F. Nawaz, M.R. Sahar, S.K. Ghoshal, A. Awang, R.J. Amjad, Judd-Ofelt analysis of spectroscopic properties of Sm3+ doped sodium tellurite glasses co-doped with Yb3+, J. Lumin. 147 (2014) 90–96. https://doi.org/10.1016/j.jlumin.2013.10.049.

[20] A. Okasha, S.Y. Marzouk, Linear and nonlinear optical properties and luminescence of Dy+3-doped aluminoborate glasses: Judd–Ofelt investigation, J. Mater. Sci. Mater. Electron. 32 (2021) 20431–20444. https://doi.org/10.1007/s10854-021-06554-6.

[21] A. Okasha, M.S. Gaafar, S.Y. Marzouk, The influence of concentration variation on the spectroscopic behavior of Sm3+-doped zinc–lead-phosphates glasses for orange and reddish-orange light-emitting applications: experimental and Judd–Ofelt approach, J. Mater. Sci. Mater. Electron. 34 (2023). https://doi.org/10.1007/s10854-022-09677-6.

[22] H.M. Elsaghier, M.A. Azooz, N.A. Zidan, W. Abbas, A. Okasha, S.Y. Marzouk, Spectroscopic and optical investigations on Er3+ ions doped alkali cadmium phosphate glasses for laser applications, J. Non. Cryst. Solids. 588 (2022) 121616. https://doi.org/10.1016/j.jnoncrysol.2022.121616.

[23] I.S. Mahmoud, M.S. Gaafar, S.Y. Marzouk, A. Okasha, H.A. Saudi, The characteristics of Nd2O3 in ZnO lead phosphate glasses regarding their mechanical, structural, and shielding properties, Appl. Phys. A Mater. Sci. Process. 128 (2022) 1–18. https://doi.org/10.1007/s00339-022-06066-y.

[24] H.M. Elsaghier, M.A. Azooz, N.A. Zidan, W. Abbas, A. Okasha, S.Y. Marzouk, The influence of Er3+ ions on the spectroscopic and lasing characteristics of alkaline earth titanium borate glasses for photonic applications, Opt. Mater. (Amst). 131 (2022) 112624. https://doi.org/10.1016/j.optmat.2022.112624.

[25] A. Okasha, A.M. Abdelghany, S.Y. Marzouk, The influence of Ba^{2+} and Sr^{2+} ions with the Dy^{3+} ions on the optical properties of lead borate glasses: Experimental and Judd-Ofelt comparative study, J. Mater. Res. Technol. 9 (2020). https://doi.org/10.1016/j.jmrt.2019.10.029.

[26] N.Y.M. Isa, E.S. Sazali, R. Hisam, S.K. Ghoshal, S.K.M. Zain, N.H. Juma'In, S.N.S. Yaacob, Z.A.S. Mahraz, A.N. Harun, F.M. Noor, M.R. Sahar, K.A. Samah, M.S. Aziz, A.A. Salim, A. Awang, Physical, Structural, and Raman Spectroscopic Traits of Neodymium-Doped Lead Oxyfluoride Zinc Phosphate Glass, J. Phys. Conf. Ser. 1892 (2021). https://doi.org/10.1088/1742-6596/1892/1/012027.

[27] C.E. Smith, R.K. Brow, The properties and structure of zinc magnesium phosphate glasses, J. Non. Cryst. Solids. 390 (2014) 51–58. https://doi.org/10.1016/j.jnoncrysol.2014.02.010.

[28] S. Jana, S. Mitra, Compositional dependence of the luminescence properties of Nd3+ ions in lead phosphate glasses: The efficient laser active materials, Opt. Laser Technol. 141 (2021) 107123.

https://doi.org/10.1016/j.optlastec.2021.107123.
[29] Q. Yin, S. Kang, X. Wang, S. Li, D. He, L. Hu, Effect of PbO on the spectral and thermo-optical properties of Nd3+-doped phosphate laser glass, Opt. Mater. (Amst). 66 (2017) 23–28. https://doi.org/10.1016/j.optmat.2017.01.036.
[30] G.N. Hemantha Kumar, J.L. Rao, K. Ravindra Prasad, Y.C. Ratnakaram, Fluorescence and Judd-Ofelt analysis of Nd3+ doped P2O5-Na2O-K2O glass, J. Alloys Compd. 480 (2009) 208–215. https://doi.org/10.1016/j.jallcom.2009.02.033.
[31] K. Linganna, C.S.D. Viswanath, R. Narro-Garcia, S. Ju, W.T. Han, C.K. Jayasankar, V. Venkatramu, Thermal and optical properties of Nd3+ ions in K-Ca-Al fluorophosphate glasses, J. Lumin. 166 (2015) 328–334. https://doi.org/10.1016/j.jlumin.2015.05.024.
[32] G. Kilic, Role of Nd3+ ions in TeO2–V2O5–(B2O3/Nd2O3) glasses: structural, optical, and thermal characterization, J. Mater. Sci. Mater. Electron. 31 (2020) 12892–12902. https://doi.org/10.1007/s10854-020-03842-5.
[33] B. V. Padlyak, R. Lisiecki, T.B. Padlyak, V.T. Adamiv, Spectroscopy of Nd3+ luminescence centres in Li2B4O7:Nd, LiCaBO3:Nd, and CaB4O7:Nd glasses, J. Lumin. 198 (2018) 183–192. https://doi.org/10.1016/j.jlumin.2018.02.046.
[34] M.S. Gaafar, S.Y. Marzouk, I.S. Mahmoud, M. Afifi, A.M. Abd El-Aziz, H. ElRashidy, Optical properties and laser prediction of strontium bismuth borate glasses doped with neodymium Ions, Phys. Scr. 96 (2021). https://doi.org/10.1088/1402-4896/ac0f40.
[35] A.K. Yadav, P. Singh, A review of the structures of oxide glasses by Raman spectroscopy, RSC Adv. 5 (2015) 67583–67609. https://doi.org/10.1039/c5ra13043c.
[36] C. Ivascu, A. Timar Gabor, O. Cozar, L. Daraban, I. Ardelean, FT-IR, Raman and thermoluminescence investigation of P2O 5-BaO-Li2O glass system, J. Mol. Struct. 993 (2011) 249–253. https://doi.org/10.1016/j.molstruc.2010.11.047.
[37] I. Ardelean, Dorina Rusu, C. Andronache, V. Ciobotă, Raman study of xMeO·(100-x)[P2O5·Li2O] (MeO⇒Fe2O3 or V2O5) glass systems, Materials Letters 61 (2007) 3301–3304
[38] G. Le Saoût, P. Simon, F. Fayon, A. Blin, Y. Vaills, Raman and infrared study of (PbO)x(P2O5)(1-x) glasses, J. Raman Spectrosc. 33 (2002) 740–746. https://doi.org/10.1002/jrs.911.
[39] Raman spectroscopy of β-irradiated aluminum-iron phosphate glass. Journal of Molecular Structure 1258 (2022) 132605.
[40] I. Shaltout, Y. Badr, Manifestation of Nd ions on the structure, Raman and IR spectra of (TeO2-MoO-Nd2O3) glasses, J. Mater. Sci. 40 (2005) 3367–3373. https://doi.org/10.1007/s10853-005-2845-3.
[41] D. Ramachari, L. Rama Moorthy, C.K. Jayasankar, Optical absorption and emission properties of Nd3+-doped oxyfluorosilicate glasses for solid state lasers, Infrared Phys. Technol. 67 (2014) 555–559. https://doi.org/10.1016/j.infrared.2014.09.020.
[42] C.R. Kesavulu, H.J. Kim, S.W. Lee, J. Kaewkhao, N. Wantana, E. Kaewnuam, S. Kothan, S. Kaewjaeng, Spectroscopic investigations of Nd3+doped gadolinium calcium silica borate glasses for the NIR emission at 1059 nm, J. Alloys Compd. 695 (2017) 590–598. https://doi.org/10.1016/j.jallcom.2016.11.002.